Molecular Catalysis 476 (2019) 110517

Contents lists available at ScienceDirect

Molecular Catalysis

journal homepage: www.elsevier.com/locate/mcat

Improving the activity and enantioselectivity of *Pv*EH1, a *Phaseolus vulgaris* epoxide hydrolase, for *o*-methylphenyl glycidyl ether by multiple site-directed mutagenesis on the basis of rational design

Chuang Li[a,1], Ting-Ting Kan[b,1], Die Hu[c], Ting-Ting Wang[b], Yong-Jun Su[b], Chen Zhang[b], Jian-Qing Cheng[c], Min-Chen Wu[c,*]

[a] Key Laboratory of Carbohydrate Chemistry and Biotechnology, Ministry of Education, School of Biotechnology, Jiangnan University, Wuxi, 214122, China
[b] School of Pharmaceutical Science, Jiangnan University, Wuxi, 214122, China
[c] Wuxi School of Medicine, Jiangnan University, Wuxi, 214122, China

ARTICLE INFO

Keywords:
*Pv*EH1
Catalytic property
Site-directed mutagenesis
Rational design
Kinetic resolution

ABSTRACT

Substrate spectrum assay exhibited that *Pv*EH1, which is an epoxide hydrolase from *P. vulgaris*, had the highest specific activity and enantiomeric ratio (*E*) for racemic *o*-methylphenyl glycidyl ether (*rac*-**1**) among tested aryl glycidyl ethers (**1**–**5**). To produce (*R*)-**1** via kinetic resolution of *rac*-**1** efficiently, the catalytic properties of *Pv*EH1 were further improved on the basis of rational design. Firstly, the seven single-site variants of *Pv*EH1-encoding gene (*pveh1*) were PCR-amplified as designed, and expressed in *E. coli* BL21(DE3). Among all expressed single-site mutants, *Pv*EH1^{L105I} and *Pv*EH1^{V106I} had the highest specific activities of 17.6 and 16.4 U/mg protein, respectively, while *Pv*EH1^{L196D} had an enhanced *E* value of 9.2. Secondly, to combine their respective merits, one triple-site variant, *pveh1*$^{L105I/V106I/L196D}$, was also amplified, and expressed. The specific activity, *E* value, and catalytic efficiency of *Pv*EH1$^{L105I/V106I/L196D}$ were 23.1 U/mg, 10.9, and 6.65 mM^{-1} s^{-1}, respectively, which were 2.0-, 1.8- and 2.4-fold higher than those of wild-type *Pv*EH1. The source of *Pv*EH1$^{L105I/V106I/L196D}$ with enhanced *E* value for *rac*-**1** was preliminarily analyzed by molecular docking simulation. Finally, the scale-up kinetic resolution of 100 mM *rac*-**1** was conducted using 5 mg wet cells/mL *E. coli*/*pveh1*$^{L105I/V106I/L196D}$ at 25 °C for 1.5 h, producing (*R*)-**1** with 95.0% ee_s, 32.1% yield and 3.52 g/L/h space-time yield.

1. Introduction

Chirality is a new emerging challenge for pharmaceutical development given that (*R*)- and (*S*)-enantiomers of a racemic drug generally exhibit different or even antagonistic pharmacological activities [1]. In view of the so-called 'chiral switch' from racemates to single enantiomers advocated by the US Food and Drug Administration (FDA) since the early 1990s, an increasing demand for enantiopure intermediates to synthesize chiral compounds has been observed [2]. Enantiopure epoxides, which are highly value-added and versatile synthons, have been diffusely applied in pharmaceutical, agrochemical and fine chemical industries [3]. For example, (*R*)-**1** is an essential chiral building block for a series of benzazepinone derivatives, which can be clinically used as β-adrenoreceptor antagonists to treat hypertension and angina pectoris [4].

Several chemical-based approaches, such as Jacobsen's asymmetric epoxidation and kinetic resolution, have been developed to prepare enantiopure epoxides, in which the expensive chiral ligands and hazardous heavy metals are required [5,6]. Considering the ever-increasing environmental awareness, biocatalysis by using whole resting cells or enzymes — an environment-friendly process with high stereoselectivity and little or no byproducts, is an attractive supplement or alternative to chemocatalysis [7]. For example, the kinetic resolution of epoxides by epoxide hydrolases (EHs; EC 3.3.2.-) provided a promising strategy to produce chiral epoxides because EHs are ubiquitous in nature, cofactor-independent, and capable of operating in organic/aqueous biphasic system [8]. Single epoxide enantiomers can be retained from their corresponding racemates with a theoretical yield of 50% via EH-catalyzed kinetic resolution [9]. However, the industrialized application of these EHs was restricted by the low activity and enantioselectivity (i.e., *E* value) [10]. Therefore, excavating novel EHs with superior catalytic properties or modifying some local

* Corresponding author.
E-mail address: biowmc@126.com (M.-C. Wu).
[1] C. Li and T.-T. Kan, the two first authors, contributed equally to this work.

https://doi.org/10.1016/j.mcat.2019.110517
Received 5 March 2019; Received in revised form 15 July 2019; Accepted 15 July 2019

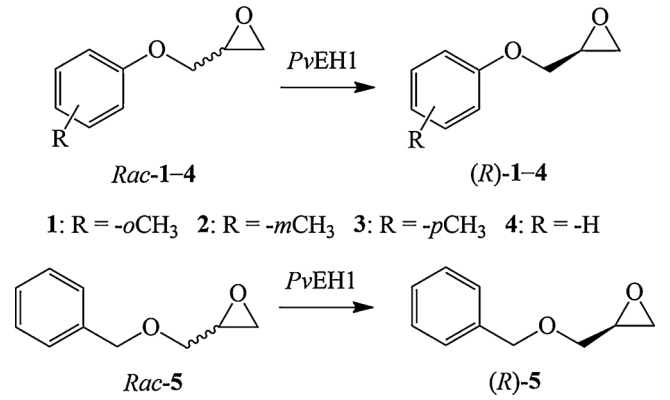

Fig. 1. Substrate spectrum assay of *Pv*EH1 for five *rac*-aryl glycidyl ethers (*rac*-**1**–**5**). **1**, *o*-methylphenyl glycidyl ether; **2**, *m*-methylphenyl glycidyl ether; **3**, *p*-methylphenyl glycidyl ether; **4**, phenyl glycidyl ether; **5**, benzyl glycidyl ether.

structures of existing EHs by protein engineering is necessary [11].

The laboratory-directed evolution of an *Aspergillus niger* EH (*An*EH) was conducted to improve its *E* value for *rac*-**4**. After one round of error-prone PCR, an *An*EH mutant (IS002B1), whose *E* value increased to 10.8 from 4.6, was selected [12]. In another example, an *Agrobacterium radiobacter* EH (*Ar*EH) was subjected to iterative saturation mutagenesis. Through screening, the best mutant, that is, T247 K/I108 L/D131S, was obtained. Its catalytic efficiency (k_{cat}/K_m) and *E* value for *rac*-epichlorohydrin were 4.5- and 2.1-fold higher than those of wild-type *Ar*EH, respectively [10]. The directed structural modification of EHs on the basis of rational design also provides additional insight into the molecular mechanism [13].

Previously, *pveh1* (GenBank: KR604729) was cloned from *P. vulgaris* total mRNA, and expressed in *E. coli* BL21(DE3). The enantioconvergent hydrolysis of styrene epoxides by *Pv*EH1 or its best mutant was studied [14]. In the present work, *Pv*EH1 had the highest specific activity and *E* value for *rac*-**1** among tested five common *rac*-aryl glycidyl ethers, which were abbreviated to *rac*-**1**–**5** in this work (Fig. 1 and Table 1). To improve the catalytic properties of *Pv*EH1 for *rac*-**1** further, a total of eight variant genes were constructed by two-stage whole-plasmid PCR on the basis of rational design. The specific activities and *E* values of the purified *Pv*EH1 and its mutants were measured, and compared. The kinetic parameters of the best mutant, that is, *Pv*EH1$^{L105I/V106I/L196D}$, were also measured. The source of its enhanced *E* value was analyzed by molecular docking (MD) simulation. The kinetic resolution of *rac*-**1** at elevated concentration was also performed using whole resting cells of *E. coli/pveh1*$^{L105I/V106I/L196D}$.

2. Experimental

2.1. Strains, plasmids, and chemicals

E. coli BL21(DE3) (Novagen, Madison, WI, USA) was used for EH expression, while PrimeSTAR HS DNA polymerase and *Dpn* I endonuclease (TaKaRa, Dalian, China) were for the site-directed mutagenesis of *Pv*EH1. Two recombinant plasmids, namely, pET-28a-*pveh1* and -*pveh1*$^{L105I/V106I}$, and one transformant expressing *Pv*EH1, designated *E. coli/pveh1*, were constructed, and preserved in our laboratory. *Rac*-**1**–**5** were purchased from TCI (Shanghai, China).

Table 1
Substrate spectrum assay of the purified *Pv*EH1 for *rac*-**1**–**5**.

Substrate	Enantiopreference	Specific activity (U/mg protein)	*E* value
Rac-**1**	(*S*)-**1**	11.7 ± 0.4	6.1
Rac-**2**	(*S*)-**2**	2.4 ± 0.1	3.0
Rac-**3**	(*S*)-**3**	2.0 ± 0.1	2.7
Rac-**4**	(*S*)-**4**	4.3 ± 0.2	3.4
Rac-**5**	(*S*)-**5**	1.8 ± 0.1	2.3

2.2. Expression and purification of PvEH1 or its mutant

A single colony of *E. coli* transformant, such as *E. coli/pveh1* or */pveh1*$^{L105I/V106I/L196D}$, was aerobically inoculated into LB medium containing 100 μg/mL kanamycin sulfate, and cultured at 37 °C for 12–14 h as the seed culture. Then, the same fresh medium was inoculated with 2% (v/v) seed culture, and cultured until the OD_{600} value reached 0.6–0.8. The expression of *Pv*EH1 or its mutant was induced by 0.2 mM IPTG at 20 °C for 10 h. The induced *E. coli* transformant cells were harvested by centrifugation, and resuspended in 50 mM NaH_2PO_4–Na_2HPO_4 buffer (pH 7.0). *E. coli* transformant harboring pET-28a(+), designated *E. coli*/pET-28a, was used as a negative control. The recombinantly expressed *Pv*EH1 or its mutant having a 6 × His tag at its N-terminus was purified by affinity chromatography using a nickel-nitrilotriacetic acid (Ni-NTA) column (Tiandz, Beijing, China). Enzyme purification and protein assay were performed as previously described [15].

2.3. EH activity assay

The activities of *Pv*EH1 and its mutants for *rac*-**1** were determined as previously described [9], with slight modification. In detail, a total of 475 μL EH solution or cell suspension, which was suitably diluted with 50 mM phosphate buffer (pH 7.0), was preincubated at 25 °C for 10 min. The reaction was initiated by adding 25 μL 200 mM (at a final concentration of 10 mM) methanol-dissolved *rac*-**1**, incubated for 10 min, and terminated by adding 2 mL methanol. The sample was analyzed by HPLC, using an e2695 apparatus (Waters, Milford, MA) equipped with an XBridge C18 column. The mobile phase, H_2O/methanol (3:7, v/v), was used at a flow rate of 0.8 mL/min, and monitored using a 2489 UV–Vis detector at 220 nm. One unit (U) of EH activity was defined as the amount of purified EH or whole resting cells hydrolyzing 1 μmol *rac*-**1** per minute under the given assay conditions. Correspondingly, the activities of *Pv*EH1 for *rac*-**2**–**5** were measured by replacing *rac*-**1** with each of them.

2.4. EH enantioselectivity assay

EH enantioselectivity, which is quantitatively described by *E* value, was used to evaluate the preferential hydrolytic degree of one enantiomer over its antipode [9]. The *E* value of *Pv*EH1 or its mutant was measured as follows: 1.8 mL suitably diluted purified EH solution and 200 μL 200 mM (at a final concentration of 20 mM) *rac*-**1**, **2**, **3**, **4** or **5** were mixed, and then incubated at 25 °C. Aliquots of 100 μL reaction sample were drawn out at different time points, extracted with 400 μL ethyl acetate, and analyzed by HPLC equipped with a Chiralcel OD-H column (Daicel, Osaka, Japan) under the same analytical conditions as stated above, except for isopropanol/*n*-hexane (2:8, v/v) as a mobile phase. The absolute configurations of single enantiomeric **1**–**5** were judged by comparing their retention times with those reported previously [16]. The conversion ratio (*c*) of substrate was calculated based on its depleted concentration. The ee_s of retained epoxide enantiomer was obtained using the following equation: $ee_s = [(R - S)/(R + S)] \times 100\%$, where *R* and *S* were the concentrations of (*R*)- and (*S*)-aryl glycidyl ether. On the basis of these parameters stated above, the *E* value was calculated from an equation: $E = \ln[(1 - c) \times (1 - ee_s)]/\ln[(1 - c) \times (1 + ee_s)]$ [17,18].

2.5. Homology modeling of PvEH1 or its best mutant

The three-dimensional (3-D) structure of *Pv*EH1 or its best mutant was homologically modeled using the MODELLER 9.11 program

(http://salilab.org/modeller/) by selecting the known crystal structure of a *Vigna radiata* EH (*Vr*EH1, PDB: 5XMD) at 2.0 Å resolution as a template, which shared 87.4% primary structure identity with *Pv*EH1. Then, the 3-D structure was subjected to molecular mechanics optimization by using the CHARMM27 force field in GROMACS 4.5 package (http://www.gromacs.org/). The outputted result with the best geometry quality was validated using the SAVES program (http://services.mbi.ucla.edu/SAVES/). Meanwhile, the 3-D structures of (*S*)- and (*R*)-**1** were handled using a ChemBio3D Ultra 12.0 software (http://www.cambridgesoft.com/).

2.6. Rational design of PvEH1 for its site-directed mutagenesis

The mutual action between the 3-D structures of *Pv*EH1 and (*S*)-**1** was predicted by MD simulation by using the AutoDock vina program (http://autodock.scripps.edu/) to locate the most appropriate binding site and steric orientation, that is, a binding state with the lowest energy. The 3-D conformation of a docked complex *Pv*EH1-(*S*)-**1** was optimized using the GROMACS 4.5 package, and then visualized using a PyMol software (http://pymol.org/) to identify the amino acid residues in proximity to (*S*)-**1** within 8 Å. Other plant EHs sharing more than 55% primary structure identity with *Pv*EH1 were searched by BLAST server in the NCBI website (http://blast.ncbi.nlm.nih.gov/). Among them, four plant EHs with superior activities and/or *E* values for *rac*-**1** were selected to conduct the multiple sequence alignment with *Pv*EH1 by using the ClustalW2 program (http://www.ebi.ac.uk/Tools/msa/clustalw2/). According to the above computer-aided analysis, the specific residues in *Pv*EH1 were selected to be separately substituted with the corresponding and frequently emerging residues (the identity is equal to 75% or 100%) among other four EHs.

2.7. Construction of E. coli transformants harboring variant genes

The single or triple site-directed mutagenesis of *pveh1* was conducted by two-stage whole-plasmid PCR as reported previously [19]. In detail, using pET-28a-*pveh1* as the template, the first-round PCR was performed with a forward primer, such as L105I-F and a reverse one (T7 terminator primer) (Table S1) under the following conditions: a denaturation at 95 °C for 4 min, followed by 30 cycles of at 98 °C for 10 s, 56 °C for 10 s, and 72 °C for 50 s. Then, the second-round PCR was carried out using the first-round PCR's product as a megaprimer: 30 cycles of at 98 °C for 10 s, 53 °C for 10 s and 72 °C for 6 min. The PCR-amplified target recombinant plasmids, such as pET-28a-*pveh1*^{L105I}, were digested by *Dpn* I to decompose the methylated template, and transformed into *E. coli* BL21(DE3), respectively, thereby constructing seven *E. coli* transformants harboring single-site variant genes, such as *E. coli/pveh1*^{L105I}. Analogously, one recombinant plasmid, pET-28a-*pveh1*$^{L105I/V106I/L196D}$, was amplified from pET-28a-*pveh1*$^{L105I/V106I}$ using a pair of primers, L196D-F and T7 terminator primer, and used for the construction of the corresponding *E. coli* transformant, that is, *E. coli/pveh1*$^{L105I/V106I/L196D}$.

2.8. Kinetic parameter assay of purified PvEH1$^{L105I/V106I/L196D}$

The initial hydrolytic rate (μmol/min/mg protein) of *rac*-**1** by *Pv*EH1$^{L105I/V106I/L196D}$ was measured under the EH activity assay conditions, except for the *rac*-**1** concentrations from 2.0 to 20.0 mM. K_m and V_{max} values were calculated by non-linear regression analysis using an Origin 9.0 software (http://www.orignlab.com/). The turnover number (k_{cat}) of EH was deduced from its apparent molecular weight and V_{max}, and its catalytic efficiency was defined as the ratio of k_{cat} to K_m.

2.9. Kinetic resolution of rac-1 at elevated concentration

Using the ee_s and yield of (*R*)-**1** as the criteria, the asymmetric hydrolytic reactions of *rac*-**1** at concentrations ranging from 50 to 120 mM were carried out in a 1 mL 50 mM phosphate buffer (pH 7.0) system, using 5 mg wet cells/mL *E. coli/pveh1*$^{L105I/V106I/L196D}$ at 25 °C for 4 h to ensure the maximum allowable concentration of *rac*-**1**. Subsequently, the scale-up kinetic resolution, in a 100 mL phosphate buffer system containing 5 mg wet cells/mL and *rac*-**1** at the maximum allowable concentration, was performed at 25 °C. During the hydrolytic process, aliquots of 100 μL reaction sample were periodically drawn out, extracted with 400 μL ethyl acetate, and then analyzed by chiral HPLC.

3. Results and discussion

3.1. Substrate spectrum assay of PvEH1

The kinetic resolution reactions of several common *rac*-aryl glycidyl ethers by various EHs, such as *Pv*EH2, *Vr*EH3 and *Tp*EH1, have been investigated [9,15,17]. In our previous studies, only the enantioconvergent hydrolysis of *rac*-styrene epoxides, such as styrene oxide, by *Pv*EH1 or its mutant was investigated [14]. Herein, to develop the industrialized application of *Pv*EH1 in the kinetic resolution of *rac*-aryl glycidyl ethers, its specific activities and *E* values for *rac*-**1**–**5** were tested, that is, the substrate spectrum assay. As shown in Table 1, the purified *Pv*EH1 enantiopreferentially hydrolyzed the (*S*)-enantiomers of all tested *rac*-**1**–**5**, and possessed the highest specific activity of 11.7 U/mg protein and *E* value of 6.1 for *rac*-**1**, suggesting that the different aryl groups in aryl glycidyl ethers significantly influenced the activity and *E* value of *Pv*EH1. However, the catalytic properties of *Pv*EH1, especially the *E* value, were still unsatisfactory for efficiently preparing (*R*)-**1** via the kinetic resolution of *rac*-**1**. Therefore, substituting several specific residues in *Pv*EH1 by single or multiple site-directed mutagenesis on the basis of computer-aided design is necessary for improving its activity and *E* value.

3.2. Specific residues selection in PvEH1

To improve the enantioselectivity of *Pv*EH1 for *rac*-**1**, that is, the enantiopreference for (*S*)-**1** efficiently, a total of 51 amino acid residues in proximity to (*S*)-**1** within 8 Å were first confirmed using a visualized PyMol software on the basis of 3-D conformation of a docked complex *Pv*EH1-(*S*)-**1**. Then, according to the result of the multiple sequence alignment of *Pv*EH1 with other four selected plant-derived EHs, 32 absolutely conserved residue sites in *Pv*EH1 were eliminated from 51 ones (Fig. 2A). After further consideration of the remaining 19 non-conserved residue sites, 12 ones can be excluded: the highest residue identities among other four plant EHs were only 50% at six sites (such as Leu^{129} and Thr^{178}), meanwhile, at the six other sites, the highest identity residues were the same as those of *Pv*EH1, such as Val^{138} and Ala^{140} (Fig. 2B). Consequently, the remaining seven specific residues, Ile^{76}, Leu^{105}, Val^{106}, Met^{175}, Leu^{196}, His^{267}, and Thr^{272}, were selected to be separately substituted with the corresponding and frequently emerging residues, Cys, Ile, Ile, Ile, Asp, Tyr, and Met, among the four other EHs (the identity is equal to 75% or 100%). The 3-D structural analysis of *Pv*EH1 displayed that Met^{175} and Leu^{196} are located in the cap domain of *Pv*EH1, whereas Ile^{76}, Leu^{105}, Val^{106}, His^{267}, and Thr^{272} are in the α/β domain (Fig. 2C). The mutations of specific residues in these two domains and near the substrate-binding pocket of EHs considerably influenced their catalytic properties [20–22].

3.3. Screening of E. coli transformants harboring single-site variants

The recombinant plasmids harboring single-site variants of *pveh1* were amplified by whole-plasmid PCR, followed by transforming them into *E. coli* BL21(DE3), respectively, thereby constructing seven corresponding *E. coli* transformants expressing *Pv*EH1 mutants, namely, *E. coli/pveh1*^{I76C}, */pveh1*^{L105I}, */pveh1*^{V106I}, */pveh1*^{M175I}, */pveh1*^{L196D},

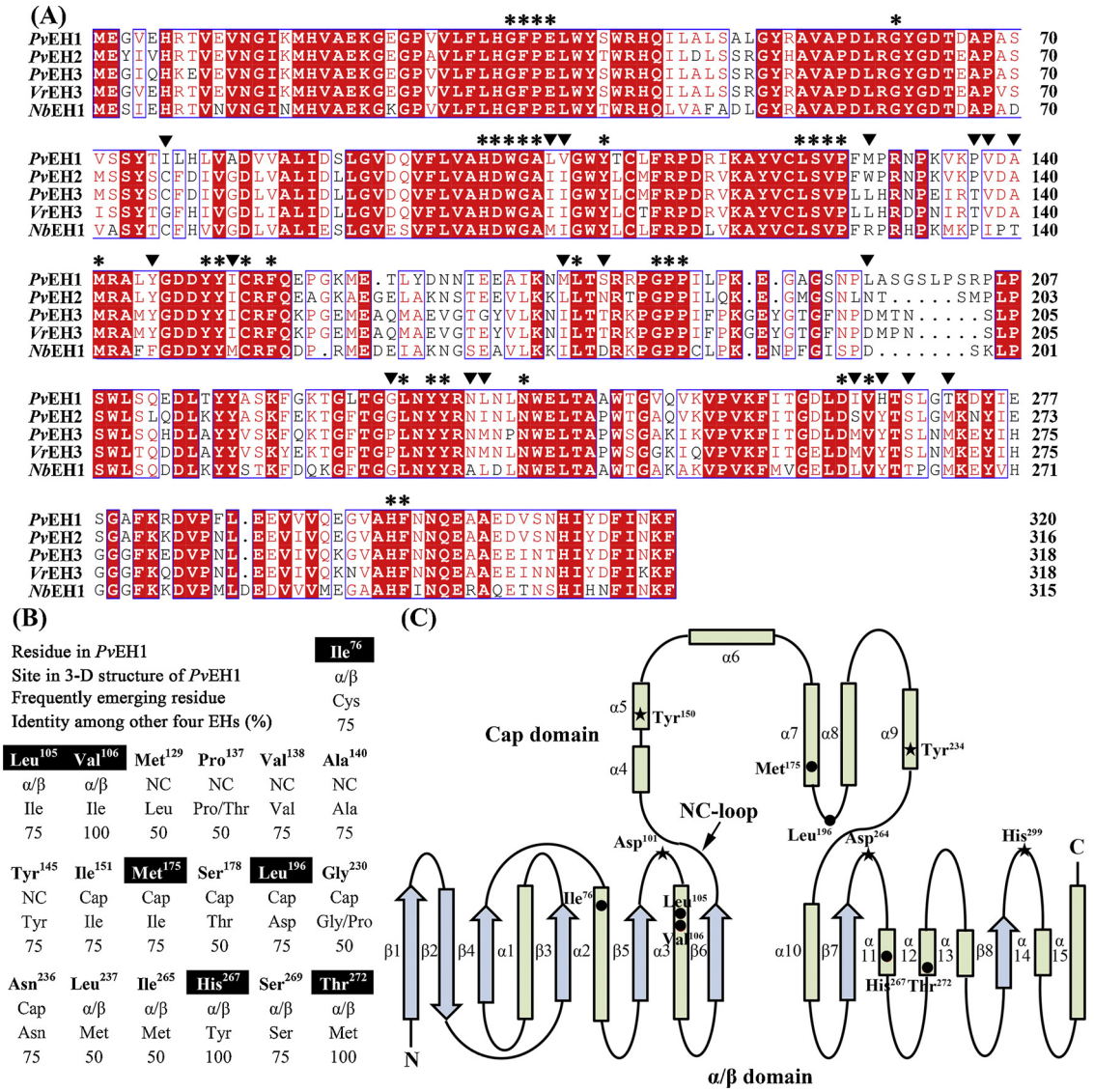

Fig. 2. Rational design of *Pv*EH1 for its site-directed mutagenesis. (A) Multiple sequence alignment of *Pv*EH1 with other four selected plant-derived EHs. *Pv*EH1 (GenBank: AKJ75509, in this work); *Pv*EH2 (ASS33914, 80.1% identity with *Pv*EH1); *Pv*EH3 (ATG22745, 71.3%); *Vr*EH3 (AKJ75505, 71.7%); *Nb*EH1 (ACE82566, 66.4%). Among the 51 residues in proximity to (*S*)-**1** within 8 Å, 32 absolutely conserved residue sites were marked with asterisks, while 19 non-conserved sites were with inverted triangles. (B) The selection of seven specific residues for the site-directed mutagenesis of *Pv*EH1. (C) The topological diagram of *Pv*EH1. The selected residue sites were marked with solid circles, while the identified sites of a catalytic triad (Asp^{101}-Asp^{264}-His^{299}) and two proton donors (Tyr^{150} and Tyr^{234}) with stars.

Table 2
Specific activities and *E* values of the purified *Pv*EH1 and its mutants for *rac*-**1**.

Enzyme	Specific activity (U/mg protein)	*E* value
*Pv*EH1	11.7 ± 0.4	6.1
*Pv*EH1^{I76C}	6.2 ± 0.3	2.3
*Pv*EH1^{L105I}	17.6 ± 0.6	7.7
*Pv*EH1^{V106I}	16.4 ± 0.5	7.5
*Pv*EH1^{M175I}	10.3 ± 0.4	5.9
*Pv*EH1^{L196D}	10.8 ± 0.5	9.2
*Pv*EH1^{H267Y}	9.0 ± 0.5	4.8
*Pv*EH1^{T272M}	6.5 ± 0.2	5.0
*Pv*EH1$^{L105I/V106I/L196D}$	23.1 ± 0.7	10.9

/pveh1^{H267Y}, and */pveh1*^{T272M}. Sodium dodecyl sulfate-polyacrylamide gel electrophoresis (SDS-PAGE) analysis displayed that the seven single-site mutants of *Pv*EH1 were successfully expressed in their respective *E. coli* transformants, such as *Pv*EH1^{L105I} in *E. coli/pveh1*^{L105I}, at 20 °C for 10 h by 0.2 mM IPTG, just the same as *Pv*EH1 expressed in *E. coli/pveh1* (as a positive control). However, no target protein band was detected in *E. coli*/pET-28a (as a negative control) under the same expression conditions (data not shown). Subsequently, the seven single-site mutants of *Pv*EH1 were purified to homogeneity, and their specific activities and *E* values for *rac*-**1** were measured (Table 2). As a result, *Pv*EH1^{L105I} and *Pv*EH1^{V106I} had the highest specific activities of 17.6 and 16.4 U/mg, which were about 1.5- and 1.4-fold higher than that (11.7 U/mg) of wild-type *Pv*EH1. Meanwhile, the *E* value of *Pv*EH1^{L196D} increased to 9.2 from 6.1 of *Pv*EH1.

3.4. Obtaining one triple-site mutant of PvEH1

A synergistic effect on the improvement in catalytic properties via combinatorial site-directed mutagenesis may be present [23]. Therefore, on the basis of above experimental results of the single site-directed mutagenesis, the three specific residues in *Pv*EH1, Leu^{105}, Val^{106}, and Leu^{196}, were subjected to a combinatorial triple site-directed mutagenesis to superimpose the superior catalytic properties of *Pv*EH1^{L105I}, *Pv*EH1^{V106I}, and *Pv*EH1^{L196D} for the kinetic resolution of *rac*-**1**. A recombinant plasmid connecting a triple-site variant, pET-28a-

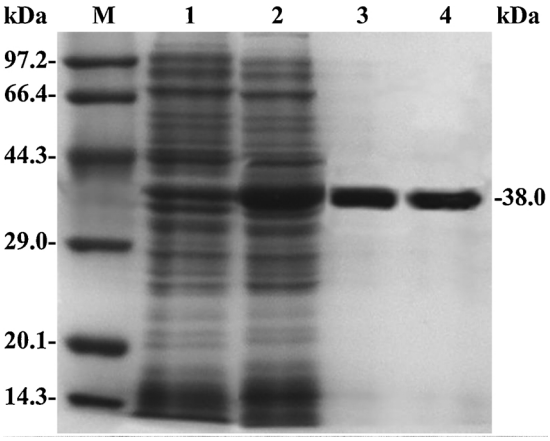

Fig. 3. SDS-PAGE analysis of the recombinantly expressed *Pv*EH1 and *Pv*EH1$^{L105I/V106I/L196D}$. Lane M, protein marker; lanes 1 and 2, the supernatants of *E. coli/pveh1* and */pveh1*$^{L105I/V106I/L196D}$ cell lysates, respectively; lanes 3 and 4, the purified *Pv*EH1 and *Pv*EH1$^{L105I/V106I/L196D}$, respectively.

pveh1$^{L105I/V106I/L196D}$, was amplified by PCR as designed theoretically, and used to construct the corresponding *E. coli* transformant, that is, *E. coli/pveh1*$^{L105I/V106I/L196D}$. The purified *Pv*EH1 and *Pv*EH1$^{L105I/V106I/L196D}$ exhibited single-target protein bands with the same apparent molecular weight of approximately 38.0 kDa (Fig. 3, lanes 3 and 4), in accordance with their respective theoretical values (37,877 and 37,893 Da) that were identified by ProtParam (http://web.expasy.org/protparam/).

As expected, *Pv*EH1$^{L105I/V106I/L196D}$ simultaneously had the highest specific activity of 23.1 U/mg and *E* value of 10.9 among all the tested single- and triple-site mutants (Table 2). Its specific activity was about 2.0-fold that of *Pv*EH1, while the EH activity (736.9 U/g wet cell) of *E. coli/pveh1*$^{L105I/V106I/L196D}$ was 4.7 folds higher than that of *E. coli/pveh1*. The EH activity assays of purified enzyme and whole resting cells, as well as SDS-PAGE analysis (Fig. 3, lanes 1 and 2) suggested that the increased soluble expression level of EH in *E. coli/pveh1*$^{L105I/V106I/L196D}$ contributed more than half to its evidently enhanced EH activity. It has been also reported that the expression levels of target enzymes in *E. coli* were elevated via site-directed mutagenesis [11,24].

3.5. Kinetic parameter of best mutant *PvEH1*$^{L105I/V106I/L196D}$

Compared with the K_m value (3.45 mM) of a wild-type *Pv*EH1, that (2.58 mM) of a triple-site mutant *Pv*EH1$^{L105I/V106I/L196D}$ decreased by 25.2%, indicating that the substrate affinity of *Pv*EH1 with *rac*-**1** (or (*S*)-**1** considering the enhanced *E* value) was improved via its triple site-directed mutagenesis. The purified *Pv*EH1 and *Pv*EH1$^{L105I/V106I/L196D}$ displayed the k_{cat} values of 9.38 and 17.15 s^{-1}, respectively. In consequence, the catalytic efficiency (6.65 mM^{-1} s^{-1}) of the latter was 2.4 times higher than that (2.72 mM^{-1} s^{-1}) of the former. These changes in kinetic parameters implied that the combinatorial substitution of L105I, V106I, and L196D in *Pv*EH1 had a remarkably positive effect on its substrate affinity and catalytic efficiency for *rac*-**1** or (*S*)-**1**.

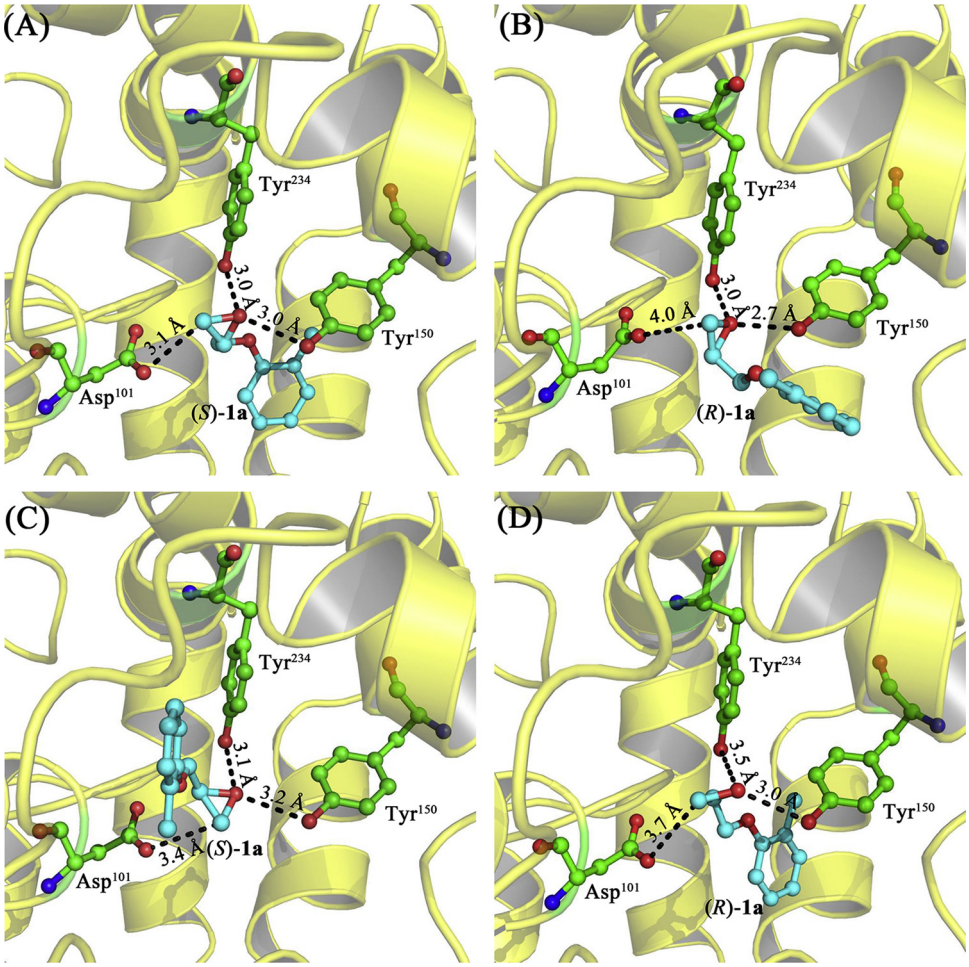

Fig. 4. Analysis of the source of *Pv*EH1$^{L105I/V106I/L196D}$ with enhanced *E* value for *rac*-**1** by MD simulation. The locally magnified 3-D conformation of a docked complex *Pv*EH1$^{L105I/V106I/L196D}$-(*S*)-**1** (A) or -(*R*)-**1** (B) was compared with that of *Pv*EH1-(*S*)-**1** (C) or -(*R*)-**1** (D).

3.6. Source of *PvEH1*$^{L105I/V106I/L196D}$ with enhanced E value

The catalytic mechanism of EHs, which are members of an α/β-hydrolase fold superfamily, was that the ring-opening of an epoxide molecule begins with the substrate activation via hydrogen bonds from two specific Tyr residues served as proton donors. Then, a nucleophilic Asp residue in the catalytic triad of EHs attacks the C_β (a less hindered C-atom in an oxirane ring) and C_α (a more hindered C-atom) with different regioselectivities [8]. In the present work, Asp^{101} in *Pv*EH1 or *Pv*EH1$^{L105I/V106I/L196D}$ was identified as a catalytic nucleophile. The C_β of (*S*)- or (*R*)-**1** was mainly attacked by Asp^{101}, affording the corresponding (*S*)- or (*R*)-diols via the retention of configuration (Fig. S1). Therefore, the through-space distance (d_β) between the nucleophilic O-atom of Asp^{101} side chain and C_β was considered as a crucial parameter [25]. To gain insight into the source of *Pv*EH1$^{L105I/V106I/L196D}$ with an enhanced *E* value, the 3-D conformations of docked *Pv*EH1$^{L105I/V106I/L196D}$-(*S*)-**1** and -(*R*)-**1** were compared with those of *Pv*EH1-(*S*)-**1** and -(*R*)-**1**, respectively (Fig. 4). The lengths (l_1 and l_2) from the hydroxyl groups of Tyr^{150} and Tyr^{234} (the proton donors in *Pv*EH1 and *Pv*EH1$^{L105I/V106I/L196D}$) to O-atom in an oxirane ring of (*S*)- or (*R*)-**1** were not more than 3.5 Å, which was the prerequisite for ring-opening reaction [15]. The d_β value of *Pv*EH1-(*S*)-**1** (or *Pv*EH1$^{L105I/V106I/L196D}$-(*S*)-**1**) was shorter than that of *Pv*EH1-(*R*)-**1** (or *Pv*EH1$^{L105I/V106I/L196D}$-(*R*)-**1**), suggesting that *Pv*EH1 or its best mutant preferentially hydrolyzes (*S*)-**1**. Although four docked complexes had approximate binding energies ranging from –18.95 to –17.47 kJ/mol, the differences in d_β values were still obvious. Through the triple site-directed mutagenesis of *Pv*EH1, the d_β to (*S*)-**1** was shortened to 3.1 from 3.4 Å, while the d_β to (*R*)-**1** increased from 3.7 to 4.0 Å. The analytical results above were in accordance with those of the experimental measurements, and similar to the conclusions drawn by other research groups [10,26,27].

3.7. Preparation of (R)-1 from rac-1 by E. coli/pveh1$^{L105I/V106I/L196D}$

The *rac*-**1** concentration (10 or 20 mM) that was used for the assay of EH activity or *E* value, was too low to realize the scale-up preparation of (*R*)-**1**. Therefore, the kinetic resolutions, in a 1 mL 50 mM phosphate buffer (pH 7.0) system containing 5 mg wet cells/mL of *E. coli/pveh1*$^{L105I/V106I/L196D}$ and *rac*-**1** at 50, 80, 100, and 120 mM were carried out, respectively, at 25 °C for 4 h. As shown in Table 3, *rac*-**1** was enantioselectively hydrolyzed up to 100 mM, retaining (*R*)-**1** with over 95.0% ee_s with only 12.0%–21.4% yield, suggesting that the excessive hydrolysis of *rac*-**1** may occur. Whereas, in the case of 120 mM *rac*-**1**, the ee_s of (*R*)-**1** was only 74.6%, and still lower than 85% even though the reaction time was prolonged to 8 h. The result indicated that substrate (*rac*-**1**) or its corresponding product (vicinal diol) at elevated concentration severely inhibited the EH activity of *E. coli/pveh1*$^{L105I/V106I/L196D}$. This phenomenon was also observed in other stereoselective hydrolytic reactions of *rac*-epoxides in an aqueous phase system by various EHs, such as *Tp*EH1 and *An*EH [17,28]. Consequently, the maximum allowable concentration of *rac*-**1** was confirmed to be 100 mM. Using whole resting cells instead of purified EH as the biocatalyst, to our knowledge, was because that the former was easily accessible, and displayed higher stability, especially at elevated substrate concentration, than the latter during the hydrolytic reaction [29].

The scale-up kinetic resolution of 100 mM *rac*-**1** catalyzed by *E. coli/pveh1*$^{L105I/V106I/L196D}$ was conducted in a 100 mL phosphate buffer system, and monitored by chiral HPLC at the given time intervals (Fig. 5). After incubation at 25 °C for 1.5 h, (*S*)-**1** was almost completely hydrolyzed at 67.0% *c* of *rac*-**1**, retaining (*R*)-**1** with 95.0% ee_s and 32.1% yield. The space-time yield (STY), which is defined as the amount of obtained target product in the unit volume and time, of (*R*)-**1** reached 3.52 g/L/h, higher than those by *An*EH- and *Tl*EH-expressing *A. niger* and *Trichosporon loubierii* resting cells [30,31], but lower than that by *E. coli* resting cells expressing *Vr*EH3 [15] (Table S2). After the hydrolytic reaction of *rac*-**1** proceeded for 3.5 h, the ee_s of (*R*)-**1** had insignificant increase, while its yield and STY obviously dropped to 23.3% and 1.02 g/L/h, respectively.

Table 3
Kinetic resolutions of *rac*-**1** at elevated concentrations by *E. coli/pveh1*$^{L105I/V106I/L196D}$.

Rac-**1** (mM)	Time (h)	*c* (%)	ee_s (%)	Yield (%)
50	4	88.2	> 95.0	12.0
80	4	81.1	> 95.0	18.7
100	4	78.0	> 95.0	21.4
120	4	57.2	74.6	37.4

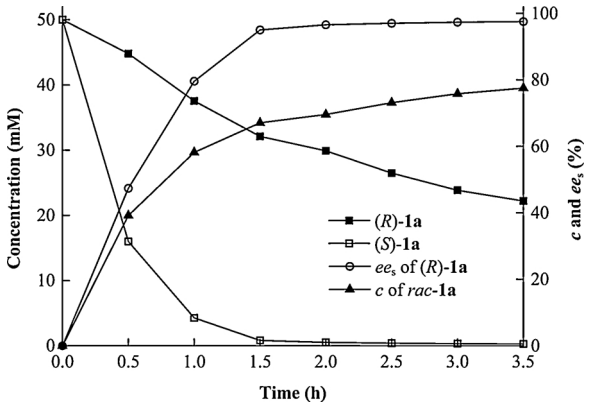

Fig. 5. Process curves of various parameters in the scale-up kinetic resolution of 100 mM *rac*-**1** at 25 °C until 3.5 h using 5 mg wet cells/mL *E. coli/pveh1*$^{L105I/V106I/L196D}$.

4. Conclusions

*Pv*EH1 showed the highest specific activity and *E* value for *rac*-**1** among five tested *rac*-aryl glycidyl ethers (**1–5**). To improve the catalytic properties, especially the *E* value, of *Pv*EH1 for *rac*-**1** efficiently, its single or triple site-directed mutagenesis was carried out on the basis of rational design. The residue substitutions of L105I and V106I in *Pv*EH1 positively affected its specific activity, while L196D enhanced its *E* value. Among all the purified *Pv*EH1 and its mutants tested, *Pv*EH1$^{L105I/V106I/L196D}$ possessed the highest specific activity and *E* value, suggesting that the combinatorial substitution of L105I, V106I, and L196D in *Pv*EH1 had a positive synergistic impact on its catalytic properties. The analytical result of *Pv*EH1$^{L105I/V106I/L196D}$ with enhanced *E* value by MD simulation was consistent with that of the experimental determination. Using whole resting cells of *E. coli/pveh1*$^{L105I/V106I/L196D}$ as the biocatalyst, the kinetic resolution of *rac*-**1** at elevated concentration was carried out, retaining (*R*)-**1** with high ee_s, yield, and STY. This work developed the application of *Pv*EH1 in the kinetic resolution of *rac*-aryl glycidyl ethers, especially the *rac*-**1**, and also provided an efficient technical strategy to customize the desired EHs for preparing target chiral epoxides.

Declaration of Competing Interest

All of the authors declare that they have no conflict of interest.

Acknowledgments

This work was financially supported by the National Natural Science Foundation of China (No. 21676117), the National First-Class Discipline Program of Food Science and Technology of China (JUFSTR20180101), and the Natural Science Foundation of Jiangsu Province for Youth of China (No. BK20180622).

Appendix A. Supplementary data

Supplementary material related to this article can be found, in the online version, at doi:https://doi.org/10.1016/j.mcat.2019.110517.

References

[1] P. Saini, D. Sareen, An overview on the enhancement of enantioselectivity and stability of microbial epoxide hydrolases, Mol. Biotechnol. 59 (2017) 98–116.

[2] J. Zaugg, Y. Gumulya, M. Bodén, A.E. Mark, A.K. Malde, Effect of binding on enantioselectivity of epoxide hydrolase, J. Chem. Inf. Model. 58 (2018) 630–640.

[3] G.S. de Oliveira, P.P. Adriani, F.G. Borges, A.R. Lopes, P.T. Campana, F.S. Chambergo, Epoxide hydrolase of *Trichoderma reesei*: biochemical properties and conformational characterization, Int. J. Biol. Macromol. 89 (2016) 569–574.

[4] A. Bisi, A. Rampa, R. Budriesi, S. Gobbi, F. Belluti, P. Ioan, E. Valoti, A. Chiarini, P. Valenti, Cardiovascular hybrid drugs: new benzazepinone derivatives as bradycardic agents endowed with selective β_1-non-competitive antagonism, Bioorg. Med. Chem. 11 (2003) 1353–1361.

[5] M. Kotik, A. Archelas, R. Wohlgemuth, Epoxide hydrolases and their application in organic synthesis, Curr. Org. Chem. 16 (2012) 451–482.

[6] M.P. Kamble, G.D. Yadav, Kinetic resolution of (*R*,*S*) phenyl glycidyl ether by red mung beans (*Vigna angularis*) epoxide hydrolases, Biocatal. Agric. Biotechnol. 12 (2017) 260–265.

[7] D. Hu, R. Wang, X.L. Shi, H.H. Ye, Q. Wu, M.C. Wu, J.J. Chu, Kinetic resolution of racemic styrene oxide at a high concentration by recombinant *Aspergillus usamii* epoxide hydrolase in an *n*-hexanol/buffer biphasic system, J. Biotechnol. 236 (2016) 152–158.

[8] E. Serrano-Hervás, M. Garcia-Borràs, S. Osuna, Exploring the origins of selectivity in soluble epoxide hydrolase from Bacillus megaterium, Org. Biomol. Chem. 15 (2017) 8827–8835.

[9] C. Li, D. Hu, X.C. Zong, C. Deng, L. Feng, M.C. Wu, Asymmetric hydrolysis of styrene oxide by *Pv*EH2, a novel *Phaseolus vulgaris* epoxide hydrolase with extremely high enantioselectivity and regioselectivity, Catal. Commun. 102 (2017) 57–61.

[10] S.P. Zou, Y.G. Zheng, Q. Wu, Z.C. Wang, Y.P. Xue, Z.Q. Liu, Enhanced catalytic efficiency and enantioselectivity of epoxide hydrolase from *Agrobacterium radiobacter* AD1 by iterative saturation mutagenesis for (*R*)-epichlorohydrin synthesis, Appl. Microbiol. Biotechnol. 102 (2018) 733–742.

[11] C. Li, J. Zhao, D. Hu, B.C. Hu, R. Wang, J. Zang, M.C. Wu, Multiple site-directed mutagenesis of a *Phaseolus vulgaris* epoxide hydrolase to improve its catalytic performance towards *p*-chlorostyrene oxide based on the computer-aided re-design, Int. J. Biol. Macromol. 121 (2019) 326–332.

[12] M.T. Reetz, C. Torre, A. Eipper, R. Lohmer, M. Hermes, B. Brunner, A. Maichele, M. Bocola, M. Arand, A. Cronin, Y. Genzel, A. Archelas, R. Furstoss, Enhancing the enantioselectivity of an epoxide hydrolase by directed evolution, Org. Lett. 6 (2004) 177–180.

[13] M. Widersten, A. Gurell, D. Lindberg, Structure-function relationships of epoxide hydrolases and their potential use in biocatalysis, BBA-Gen. Subjects 1800 (2010) 316–326.

[14] H.H. Ye, D. Hu, X.L. Shi, M.C. Wu, C. Deng, J.F. Li, Directed modification of a novel epoxide hydrolase from *Phaseolus vulgaris* to improve its enantioconvergence towards styrene epoxides, Catal. Commun. 87 (2016) 32–35.

[15] D. Hu, C.D. Tang, C. Li, T.T. Kan, X.L. Shi, L. Feng, M.C. Wu, Stereoselective hydrolysis of epoxides by re*Vr*EH3, a novel *Vigna radiata* epoxide hydrolase with high enantioselectivity or high and complementary regioselectivity, J. Agric. Food Chem. 65 (2017) 9861–9870.

[16] N. Bala, S.S. Chimni, H.S. Saini, B.S. Chadha, *Bacillus alcalophilus* MTCC10234 catalyzed enantioselective kinetic resolution of aryl glycidyl ethers, J. Mol. Catal. B Enzym. 63 (2010) 128–134.

[17] K. Wu, H.L. Wang, H.H. Sun, D.Z. Wei, Efficient kinetic resolution of phenyl glycidyl ether by a novel epoxide hydrolase from Tsukamurella paurometabola, Appl. Microbiol. Biotechnol. 99 (2015) 9511–9521.

[18] C.S. Chen, Y. Fujimoto, G. Girdaukas, C.J. Sih, Quantitative analyses of biochemical kinetic resolutions of enantiomers, J. Am. Chem. Soc. 104 (1982) 7294–7299.

[19] J. Sanchis, L. Fernández, J.D. Carballeira, J. Drone, Y. Gumulya, H. Höbenreich, D. Kahakeaw, S. Kille, R. Lohmer, J.J.-P. Peyralans, J. Podtetenieff, S. Prasad, P. Soni, A. Taglieber, S. Wu, F.E. Zilly, M.T. Reetz, Improved PCR method for the creation of saturation mutagenesis libraries in directed evolution: application to difficult-to-amplify templates, Appl. Microbiol. Biotechnol. 81 (2008) 387–397.

[20] M. Kotik, A. Archelas, V. Faměrová, P. Oubrechtová, V. Křen, Laboratory evolution of an epoxide hydrolase — towards an enantioconvergent biocatalyst, J. Biotechnol. 156 (2011) 1–10.

[21] L.F. Zhang, J.M. Wu, H. Feng, Homology modelling and site-directed mutagenesis studies of the epoxide hydrolase from Phanerochaete chrysosporium, J. Biochem. 149 (2011) 673–684.

[22] Z.T. Sun, R. Lonsdale, L. Wu, G.Y. Li, A.T. Li, J.B. Wang, J.H. Zhou, M.T. Reetz, Structure-guided triple-code saturation mutagenesis: efficient tuning of the stereoselectivity of an epoxide hydrolase, ACS Catal. 6 (2016) 1590–1597.

[23] M.T. Reetz, Biocatalysis in organic chemistry and biotechnology: past, present, and future, J. Am. Chem. Soc. 135 (2013) 12480–12496.

[24] Q. Luo, Y. Chen, J. Xia, K.Q. Wang, Y.J. Cai, X.R. Liao, Z.B. Guan, Functional expression enhancement of *Bacillus pumilus* CotA-laccase mutant WLF through site-directed mutagenesis, Enzyme Microb. Tech. 109 (2018) 11–19.

[25] M.T. Reetz, M. Bocola, L.W. Wang, J. Sanchis, A. Cronin, M. Arand, J.Y. Zou, A. Archelas, A.L. Bottalla, A. Naworyta, S.L. Mowbray, Directed evolution of an enantioselective epoxide hydrolase: uncovering the source of enantioselectivity at each evolutionary stage, J. Am. Chem. Soc. 131 (2009) 7334–7343.

[26] F. Xue, Z.Q. Liu, N.W. Wan, H.Q. Zhu, Y.G. Zheng, Engineering the epoxide hydrolase from *Agromyces mediolanus* for enhanced enantioselectivity and activity in the kinetic resolution of racemic epichlorohydrin, RSC Adv. 5 (2015) 31525–31532.

[27] Z.Q. Liu, L.P. Zhang, F. Cheng, L.T. Ruan, Z.C. Hu, Y.G. Zheng, Y.C. Shen, Characterization of a newly synthesized epoxide hydrolase and its application in racemic resolution of (*R*,*S*)-epichlorohydrin, Catal. Commun. 16 (2011) 133–139.

[28] H.X. Jin, Z.C. Hu, Y.G. Zheng, Enantioselective hydrolysis of epichlorohydrin using whole *Aspergillus niger* ZJB-09173 cells in organic solvents, J. Biosci. 37 (2012) 695–702.

[29] E.Y. Lee, M.L. Shuler, Molecular engineering of epoxide hydrolase and its application to asymmetric and enantioconvergent hydrolysis, Biotechnol. Bioeng. 98 (2007) 318–327.

[30] W.J. Choi, E.C. Huh, H.J. Park, E.Y. Lee, C.Y. Choi, Kinetic resolution for optically active epoxides by microbial enantioselective hydrolysis, Biotechnol. Tech. 12 (1998) 225–228.

[31] Y. Xu, J.H. Xu, J. Pan, Y.F. Tang, Biocatalytic resolution of glycidyl aryl ethers by *Trichosporon loubierii*: cell/substrate ratio influences the optical purity of (*R*)-epoxides, Biotechnol. Lett. 26 (2004) 1217–1221.